Measurements and modelling of I2, IO, OIO, BrO and NO3 in the mid-latitude marine boundary layer

A. Saiz-Lopez, J. A. Shillito, H. Coe, J. M. C. Plane

Atmos. Chem. Phys. Discuss., 5, 9731–9767, 2005
www.atmos-chem-phys.org/acpd/5/9731/
SRef-ID: 1680-7375/acpd/2005-5-9731
European Geosciences Union

Atmospheric Chemistry and Physics Discussions

Measurements and modelling of I_2, IO, OIO, BrO and NO_3 in the mid-latitude marine boundary layer

A. Saiz-Lopez[1], **J. A. Shillito**[2], **H. Coe**[2], **and J. M. C. Plane**[1]

[1]School of Environmental Sciences, University of East Anglia, Norwich, UK
[2]School of Earth, Atmospheric and Environmental Sciences, University of Manchester, Manchester, UK

Received: 26 August 2005 – Accepted: 4 September 2005 – Published: 10 October 2005

Correspondence to: J. M. C. Plane (j.plane@uea.ac.uk)

Abstract

Time series observations of molecular iodine (I_2), iodine oxides (IO, OIO), bromine oxide (BrO), and the nitrate radical (NO_3) in the mid-latitude coastal marine boundary layer (MBL) are reported. Measurements were made using a new long-path DOAS instrument during a summertime campaign at Mace Head on the west coast of Ireland. I_2 was detected using the $B^3\Pi(0_u^+)-X^1\Sigma_g^x$ electronic transition between 535 and 575 nm. The I_2 mixing ratio was found to vary from below the detection limit (~5 ppt) up to a nighttime maximum of 93 ppt. Along with I_2, observations of IO, OIO and NO_3 were also made during the night. Surprisingly, IO and OIO were detected at mixing ratios up to 2.5 and 10.8 ppt, respectively. A model is employed to show that the reaction between I_2 and NO_3 is the likely nighttime source of these radicals. The BrO mixing ratio varied from below the detection limit at night (~1 ppt) to a maximum of 6 ppt in the first hours after sunrise. A model shows that this diurnal behaviour can be explained by halogen recyling in sea-salt aerosol building up photolabile precursors of atomic Br during the preceding night. In the same campaign a zenith sky DOAS was employed to determine the column density variation of NO_3 as a function of solar zenith angle (SZA) during sunrise, from which vertical profiles of NO_3 through the troposphere were obtained. On several occasions a positive gradient of NO_3 was observed over the first 2 km, possibly due to dimethyl sulphide (DMS) removing NO_3 at the ocean surface.

1. Introduction

Interest in atmospheric halogen chemistry has grown enormously in the past three decades, originally because of its active role in the destruction of stratospheric (Molina and Rowland, 1974; Wofsy et al., 1975; Farman et al., 1985) and polar tropospheric (Barrie et al., 1988; Finlayson-Pitts et al., 1990; McConnell et al., 1992; Hausmann and Platt, 1994; Honninger and Platt, 2002) ozone. However, halogen radicals could play a key role in a number of other important tropospheric processes, including NO_x (NO and

ACPD
5, 9731–9767, 2005

NO_2) and HO_x (OH and HO_2) chemistry, the oxidation of a range of organic molecules, and in the formation of ultra-fine particles. These impacts are discussed in greater detail below. In the mid-latitude MBL, BrO has recently been detected both by multi-axis DOAS (Leser et al., 2003) and long-path DOAS (Saiz-Lopez et al., 2004a). The source of bromine is almost certainly the release of species such as Br_2, BrCl and IBr from sea-salt aerosol, following the uptake from the gas phase, and subsequent aqueous-phase reactions, of hypohalous acids (HOX, where X=Br, I) (Vogt et al., 1996). In semi-polluted areas with higher NO_x, the uptake of di-nitrogen pentoxide (N_2O_5), formed at night by the recombination of the NO_3 with NO_2, also leads to the release of $BrNO_2$ (Behnke et al., 1994). These heterogeneous mechanisms are supported by the observation that the bromide ions in sea-salt aerosols are substantially depleted (Ayers et al., 1999; Gabriel et al., 2002). Once released into the gas phase, these bromine-containing compounds will photolyse rapidly during the day, and the resulting Br atoms will react fast with O_3 to form BrO.

Recent measurements of IO and OIO (Alicke et al., 1999; Allan et al., 2000a, 2001; Saiz-Lopez and Plane, 2004) have confirmed the importance of iodine chemistry in the MBL. The source of atmospheric iodine is the evasion of biogenic iodocarbons such as CH_3I, CH_2I_2, CH_2IBr and CH_2ICl from both the open ocean and coastal areas (Carpenter et al., 1999). Additionally, the detection of I_2 during NAMBLEX indicates that this molecule is probably the major source of atmospheric iodine in certain coastal locations (Saiz-Lopez and Plane, 2004). Also, I_2 would account for the surprising nighttime observations of IO and OIO, since the rate constant between NO_3 and I_2 to yield INO_3 and I is relatively fast (Chambers et al., 1992). The atomic I produced in this way would rapidly form IO by reaction with O_3. A number of studies have proposed iodine as a significant catalyst in tropospheric O_3 depletion (Jenkin et al., 1985; Davis et al., 1996; McFiggans et al., 2000). BrO and IO also compete effectively with the OH radical in the oxidation of DMS (Saiz-Lopez et al., 2004a; Glasow and Crutzen, 2004), and a very recent study has shown that the HO_2/OH ratio in the coastal MBL is significantly altered by IO (Bloss et al., 2005). Another potentially significant aspect of the iodine

chemistry is the condensation of iodine oxide vapours, leading to the formation of new ultra-fine particles in the daytime marine atmosphere (O'Dowd et al., 2002; McFiggans et al., 2004; Saiz-Lopez et al., 2005).

Field observations of the NO_3 radical over the past 25 years have demonstrated that it plays a major role in the chemistry of the nighttime troposphere (Platt et al., 1980, 1990; Heintz et al., 1996; Allan et al., 2000b, 2002a; Brown et al., 2003, 2004). NO_3 reacts rapidly with DMS in the MBL (Butkovskaya and LeBras, 1994). The radical also recombines with NO_2 to establish an equilibrium with N_2O_5. The subsequent heterogeneous uptake of N_2O_5 on aqueous sea-salt aerosol both removes NO_x and activates halogens (see above).

In this paper we report results from a 5 week campaign of boundary layer observations of I_2, IO, OIO, BrO and NO_3 made by long-path differential optical absorption spectroscopy (DOAS), and measurements of the vertical concentration profiles of NO_3 by zenith sky DOAS. Box models are then used to investigate the nighttime chemistry of iodine, and the diurnal behaviour of BrO.

2. Experimental

2.1. Long-path DOAS instrument

The DOAS measurements were performed at the Mace Head Atmospheric Research Station (MHARS) on the west coast of Ireland (53°20′ N, 9°54′ W), during the NAMBLEX (North Atlantic Marine Boundary Layer EXperiment) campaign in July/August 2002. The long-path DOAS instrument was housed in an observatory on the foreshore at the MHARS. It consists of a Newtonian telescope containing the xenon arc lamp source, and the transmitting and receiving optics. The light beam was folded back to the transmitter by a retro-reflector situated 4.2 km away on Croaghnakeela Island (see Fig. 2 in Saiz-Lopez et al., 2005), providing an optical absorption path of 8.4 km, about 5–20 m above sea level. Differential absorption spectra were collected by averaging

ACPD
5, 9731–9767, 2005

for 30 min when measuring I_2, IO, OIO and BrO, or 20 min when detecting NO_3. More details on the instrument design and spectral deconvolution procedures are provided elsewhere (Plane and Saiz-Lopez, 2005). The following reference spectra were taken from the literature and adapted to the spectrometer instrument function: I_2 (Saiz-Lopez et al., 2004b), IO (Harwood et al., 1997), OIO (P. Spietz, University of Bremen, personal communication, 2005), BrO (Wahner et al., 1988) and NO_3 (Yokelson et al., 1994).

2.2. Zenith sky DOAS instrument

This instrument consists of a 0.8° field-of-view telescope, fixed in a zenith-viewing geometry and coupled to a spectrometer by means of a fibre optic cable. Spectra were recorded with a resolution of 0.5 nm in the λ=640–700 nm region for detection of NO_3. A detailed description of the instrument is given in (Allan et al., 2002a). Spectra were acquired every 1–2 min (depending on scattered light levels) for approximately 2 h through sunrise (SZA 95°). The NO_3 column abundances were obtained using the same de-convolution method as for the long-path DOAS measurements, with a reference spectrum recorded after sunrise when the NO_3 mixing ratio is negligible due to the rapid photodissociation of the radical (Allan et al., 2002a). The vertical concentration profile was then determined using an optimal estimation algorithm described below.

3. Results and discussion

3.1. Long-path DOAS measurements of NO_3

Observations of NO_3 were performed during 16 nights under different meteorological conditions. Figure 1 summarises the NO_3 time series set during the campaign. The maximum value reached during the observation period was 25 ppt, with averages of ~3 and 13 ppt for clean marine and semi-polluted air masses. These values are consistent with previously reported observations at the same location, under a similar range

ACPD
5, 9731–9767, 2005

of meteorological conditions (Allan et al., 2000b). Comparable nighttime mixing ratio profiles have been reported in other marine areas (Heintz et al., 1996; Allan et al., 1999; Brown et al., 2004; Vrekoussis et al., 2004). The significant variations in NO_3 levels during the period of measurements can be explained by considering the back trajectories of the air masses arriving in the MBL at Mace Head. Figures 2 and 3 show two different types of air masses and the associated NO_3 mixing ratios. The solid and broken grey bars correspond to sunset and sunrise, respectively. Typically, NO_3 mixing ratios below 5 ppt were associated with air masses from the Atlantic Ocean sector, Fig. 2a and b. By contrast, NO_3 mixing ratios above 10 ppt coincided with semi-polluted air masses from the UK or the European continent Fig. 3a and b. Note that although the predicted back trajectories on 3 September have their origin in the north Atlantic, the air mass has traversed over parts of the United Kingdom and the European continent before reaching Mace Head.

NO_3 is formed by the oxidation of NO_2 by O_3, with a rate constant $k(NO_2+O_3)=1.2\times 10^{-13}$ exp (-2450/T) cm^3 molecule^{-1} s^{-1} (Sander et al., 2003). In the immediate post-dusk hours, once photolysis ceases and before NO_3 builds up to a chemical steady state, assuming other losses are negligible, the rate of increase of NO_3 should just be the rate of production, $R_{NO_3}=k(NO_2+O_3)$ $[O_3][NO_2]$. Taking the observed average NO_2 and O_3 mixing ratios of 450 ppt and 22 ppb, respectively, and an average temperature of 288 K, then $R_{NO_3}=22$ ppt h^{-1} is obtained. This rate is in good accord with the observations (see Fig. 3a). We have shown previously that under clean marine air conditions at Mace Head during summer, DMS controls the removal of NO_3, whereas in semi-polluted air masses NO_3 removal is dominated by the indirect loss of N_2O_5 (Allan et al., 2000b).

During NAMBLEX the broad-band cavity ring-down spectroscopy (BBCRDS) technique was also employed to make in-situ measurements of the NO_3 radical. An intercomparison of the local and long-path observations can be found in Bitter et al. (2005)[1].

[1]Bitter, M., Ball, S. M., Povey, I. M., Jones, R. L., Saiz-Lopez, A., and Plane, J. M. C.:

A photochemical box model of the nighttime NO_3 chemistry (Allan et al., 2000b) was used to simulate the production of N_2O_5 from its equilibrium with NO_3. The model was run under typical westerly clean marine conditions, for which an average NO_3 mixing ratio of 3 ppt was observed. For marine air masses, the N_2O_5 accommodation coefficient in the model, γN_2O_5, was set at 0.03 (Behnke et al., 1997; Allan et al., 2000b). Under these clean marine conditions, with an aerosol volumetric surface area of 10^{-7} cm^2 cm^{-3}, the modelled N_2O_5 mixing ratio throughout the night is ~3 ppt. This N_2O_5 mixing ratio will be used in a bromine chemistry model to assess the contribution of NO_3 chemistry to halogen activation on sea-salt particles (Sect. 3.6).

3.2. Zenith sky observations of NO_3 vertical profiles

NO_3 vertical column measurements were carried out at sunrise during six days, as shown in Fig. 4. The left-hand panels (Fig. 4a) show the expected dependence of NO_3 column on SZA: as the solar terminator sweeps down through the atmosphere, more and more of the overlying NO_3 is removed by photolysis. Note that the errors associated with individual column density measurements are quite variable. These uncertainties arise mainly from the visibility conditions, and the temperature dependence of the NO_3 absorption cross-section (Allan et al., 2002a). The literature cross-section employed is that of Yokelson et al. (1994) at 280 K, a temperature which can be considered representative of the lower troposphere where the contribution to the NO_3 total absorption column should be strongest. In Fig. 4a it can be seen that the NO_3 persisted after dawn on several occasions. This effect is most likely due to the thermal decomposition of N_2O_5 competing with photolysis to sustain the NO_3 mixing ratio past sunrise (Smith and Solomon, 1990; Smith et al., 1993; Allan et al., 2002a; Coe et al., 2002).

The conversion from column abundance to vertical mixing ratio profiles was made

Measurements of NO_3, N_2O_5, OIO, I_2, water vapour and aerosol optical depth by broadband cavity ringdown spectroscopy during the NAMBLEX campaign, Atmos. Chem. Phys. Discuss., in preparation, 2005.

using the optimal estimation method (OEM) (Rodgers, 1976, 1990). Briefly, the forward model used is described by the expression $\mathbf{y}=\mathbf{Kx}$, where knowing the state of the system or weighing matrix function ($\mathbf{K}$) and the vertical mixing ratio profile ($\mathbf{x}$), the column density time series ($\mathbf{y}$) can be predicted. However, since $\mathbf{x}$ is not known the forward model is inverted to give the backward model $\mathbf{x}=\mathbf{K}^{-1}\mathbf{y}$. The inversion process makes use of 'a priori' information, i.e. the likely NO_3 vertical profile, to allow NO_3 vertical distribution information to be retrieved. $\mathbf{K}$ comprises photolysis of NO_3 as a function of height, SZA and time (Coe et al., 2002).

In Fig. 4a the predicted column abundance (solid red line) using the forward model is compared with the measured, as a function of SZA. Figure 4b illustrates the corresponding retrieved NO_3 vertical concentration profiles. These profiles exhibit strong gradients, consistent with other observations (Allan et al., 2002a). On all six days, the highest NO_3 concentrations are in the mid- to low troposphere. There are probably three reasons for this. First, higher temperatures and NO_2 concentrations will cause NO_3 to be produced more rapidly. Second, the thermal decomposition of N_2O_5 back to NO_3 will be faster. Third, DMS evading from the ocean will remove NO_3 at the base of the MBL, creating a positive gradient of NO_3 in the MBL. This probably explains the observations in clean marine conditions on 3, 7 and 10 August. On the night of 2 August (when the site was influenced by semi-polluted continental air masses) long-path DOAS and zenith sky measurements of NO_3 were performed simultaneously. In Fig. 4b (top panel) the boundary layer measurement of ~10 ppt just before dawn is comparable to the 7 ppt retrieved for the lowest box in the vertical profile, which is centred at 2 km. On 9 and 11 August, back trajectories show boundary layer air arriving after traversing north-south along the west coast of Ireland, which probably accounts for the relatively high NO_3 concentrations in the lowest box.

3.3. Iodine species (I_2, IO, OIO)

Figure 5 illustrates the time series of I_2, IO and OIO during NAMBLEX. The broken line in each of the panels shows the average DOAS detection limit for the particular

species during the campaign. Measurements of I_2 were carried out during 18 days. As we have demonstrated in an accompanying paper (Saiz-Lopez et al., 2005), the photolysis lifetime of I_2 is so short (~15 s) that during daytime I_2 is very inhomogeneously distributed along the DOAS light path. Thus the daytime mixing ratios of I_2 (and IO) in Fig. 5 should be treated with caution – they are useful as relative rather than absolute measurements. The maximum I_2 mixing ratio observed during the campaign was 93 ppt. This was observed at night, when the average I_2 mixing ratio was considerably higher, as expected in the absence of photolysis.

Figure 5 shows that the I_2 mixing ratio is characterised by sharp peaks lasting for 30 to 45 min. These peaks always coincided with low tide (Saiz-Lopez and Plane, 2004). Indeed, a simple plot of I_2 mixing ratio versus tidal height exhibits a clear anti-correlation, as shown in Fig. 6. The source of I_2 at this coastal environment is almost certainly macro-algae (e.g. *Laminaria*), which accumulate iodine compounds well over the concentration of such chemical species in seawater, leading to direct injection of I_2 when the plant is exposed to the atmosphere at low tide (Truesdale et al., 1995; Kupper et al., 1998; McFiggans et al., 2004). The role of I_2 in the production of new particles in coastal areas has been recently proposed by Saiz-Lopez and Plane (2004) and McFiggans et al. (2004), and explored in detail using an iodine chemistry model (Saiz-Lopez et al., 2005). These studies show that I_2 is the major contributor to the particle bursts observed at Mace Head.

In contrast to the state of the tide, the I_2 mixing ratio did not correlate significantly with local wind direction. This is not surprising since the prevailing wind directions tended to be westerly or easterly, and macroalgae were exposed at both ends of the light path (see the map in Saiz-Lopez et al., 2005). Nevertheless, one potentially interesting detail is that I_2 was observed at night in westerly winds, irrespective of the state of the tide. This may indicate that I_2 is also produced over the open ocean, as originally proposed by Garland and Curtis (1981).

Figure 5 also shows the complete time series of IO during NAMBLEX, totalling 15 days of measurements. The maximum IO mixing ratio during the campaign was ~7 ppt,

measured during daytime. This is in accord with previously reported IO observations at Mace Head (Alicke et al., 1999; Allan et al., 2000a). Note that this mixing ratio is probably the average of a rather inhomogeneous distribution along the DOAS path (Saiz-Lopez et al., 2005). During daytime, IO exhibited a clear anti-correlation with tidal height and solar irradiation, as shown in the mesh plot in Fig. 7. This is good evidence for its photochemical production from coastal emissions of I_2 (Saiz-Lopez and Plane, 2004). IO was only measured during two nights of NAMBLEX, when mixing ratios up to ~2.5 ppt were observed.

OIO measurements were made simultaneously with I_2 in the 535–575 nm wavelength region. During the day, OIO was not observed above the daytime detection limit of ~4 ppt. The radical was only observed at night, with a maximum mixing ratio of 10.8 ppt. In fact, on this occasion the OIO peaked after local midnight, and about 2 h after a night-time peak of I_2 at low tide (Saiz-Lopez and Plane, 2004). The observation that OIO is only detectable at night is consistent with previous measurements made by us at Cape Grim (Tasmania), another remote marine location (Allan et al., 2001).

There appear to be two possible explanations for the absence of OIO during daytime. First, it could photolyse following absorption in the strong bands between about 470 and 610 nm. Whilst certain experimental evidence led us to conclude this was the case (Ashworth et al., 2002), we have recently shown that absorption leads to interconversion into the highly vibrationally-excited ground state rather than dissociation to $I+O_2$, so the quantum yield for photolysis is probably much less than 10% at 562 nm (D. M. Joseph, S. H. Ashworth, and J. M. C. Plane, University of East Anglia, personal communication). Nevertheless, a small probability of photolysis, integrated over the absorption bands, could still account for the removal of OIO during daytime (Saiz-Lopez et al., 2005). A second possibility is that OIO is removed during daytime by reaction with radicals that have marked diurnal cycles with daytime maxima, such as OH, NO and IO. Based on our current experimental and theoretical work, we believe that the most likely of these is IO, as discussed in our recent modelling study (Saiz-Lopez et al., 2005).

ACPD
5, 9731–9767, 2005

3.4. Nighttime iodine chemistry

In order to understand the source of IO and OIO during the night in the MBL, we have modified our existing iodine chemistry model (McFiggans et al., 2000; Saiz-Lopez et al., 2005). A plausible mechanism for the formation of atomic iodine at night is the reaction of $I_2+NO_3 \rightarrow INO_3+I$, which has a rate constant at 295 K of 1.5×10^{-12} cm^3 molecule^{-1} s^{-1} (Chambers et al., 1992). The resulting I atom would form IO in the atmosphere, and a simple calculation showed that this reaction might be fast enough to account for the nighttime observations of IO (Saiz-Lopez and Plane, 2004). The other product is INO_3. Assuming an accommodation coefficient, γINO_3, of 0.05 and a clean MBL aerosol volumetric surface area of 10^{-7} cm^2 cm^{-3}, the loss rate due to uptake on aerosols is $\sim2.3\times10^{-5}$ s^{-1}. An upper limit to the rate of thermal dissociation at 285 K has been determined to be 4.5×10^{-4} s^{-1} (Allan and Plane, 2002b). Hence, at night in the MBL there will be a competition between uptake on aerosols and thermal decomposition of INO_3.

We also consider in the model the thermal stabilities of I_2O_2 and I_2O_4, dimers that form from the self reactions of IO and OIO, respectively. Ab initio quantum calculations, using a level of theory described previously (Allan and Plane, 2002b), show that the binding energy of the OIO dimer is only 72 kJ mol^{-1}, while that of the IO dimer (in the form IOIO) is about 86 kJ mol^{-1}. Using these binding energies, vibrational frequencies and rotational constants as input for a Rice-Ramsberger-Kassel-Markus (RRKM) calculation, we predict that the rates of dissociation of these dimer molecules will be fast at a typical mid-latitude MBL nighttime temperature of 285 K and a pressure of 1 atmosphere. I_2O_4 will dissociate back to OIO+OIO at a rate of $\sim7\times10^3$ s^{-1}. IOIO will dissociate to OIO+I and IO+IO at rates of ~12 and 4 s^{-1}, respectively. The atmospheric implication of these results will be a delay in the rate of disappearance of IO and OIO in the nighttime MBL. These dissociation rates, and the rate constant for the association of the OIO dimer (predicted from RRKM theory to be $\sim5\times10^{-11}$ cm^3 molecule^{-1} s^{-1} at 1 atm and 285 K), are included in the model.

ACPD
5, 9731–9767, 2005

When running the model, the source of I_2 was constrained to produce the average nighttime I_2 peak of about 40 ppt that was observed during nocturnal low tide. The rate of I_2 emission in the model followed a Gaussian distribution, peaking at low tide, with a standard width of 22 min (Saiz-Lopez et al., 2005). The NO_3 mixing ratio was fixed at 10 ppt. Figure 8a shows the time- profiles of I_2, IO and OIO. The O_3 profile is also shown, although the predicted O_3 loss rate is negligible (3×10^{-2} ppb h^{-1}). In the absence of photolysis, the I_2 peak decays much more slowly than during the day, in accord with our observations (Saiz-Lopez and Plane, 2004).

In this model run the IO and OIO mixing ratios peak at 2 ppt and 1.7 ppt, respectively, coincident with low tide. Hence, there are two things that differ from the nighttime observations. First, the OIO/IO ratio predicted by the model is 0.9, whereas the measurements indicate that this ratio is ~4. Second, the observations show that the OIO peak occurs after I_2 reaches its maximum at low tide. Therefore, to reconcile the measurements with the model results, another route for converting IO to OIO, in addition to the self reaction of IO, is required. Although the reaction $IO+O_3 \rightarrow OIO+O_2$ is exothermic by about 150 kJ mol^{-1} (Misra and Marshall, 1998), a very small upper limit to the rate constant of 10^{-15} cm^3 molecule^{-1} s^{-1} has been determined (Atkinson et al., 2000), so that this reaction would be too slow. Another candidate is the reaction:

$$IO + NO_3 \rightarrow OIO + NO_2 \quad (1)$$

Although this reaction does not appear to have been studied, it is also exothermic (by about 50 kJ mol^{-1}), and NO_3 is in general a more aggressive reactant than O_3: for instance, it reacts about 10^5 times faster with I_2.

When Reaction (1) is included in the model, the rate constant needs to be larger than 7×10^{-12} cm^3 molecule^{-1} s^{-1} in order to increase the modelled OIO/IO ratio to the observed ratio of 4. This model run is shown in Fig. 8b; note that the OIO peak now occurs after the maxima of I_2 and IO, as observed. Although this model does not include vertical mixing or consider inhomogeneity along the DOAS light path when comparing with the observations, it does include the uptake of OIO (and IO) onto a background

ACPD
5, 9731–9767, 2005

aerosol loading typical of Mace Head (Saiz-Lopez et al., 2005). We therefore consider the level of agreement with the observations to be encouraging. A study of Reaction (1) appears to be a priority to develop further understanding of nighttime iodine chemistry.

3.5. BrO observations

BrO was measured over 6 days during NAMBLEX (Saiz-Lopez et al., 2004a). A maximum mixing ratio of 6 ppt was observed, coinciding with westerly and relatively high speed winds (up to 11 m s^{-1}), whereas a mean daytime mixing ratio of 2.3 ppt was observed. The diurnal profile was characterised by a short-lived pulse after dawn. Figure 9 shows an average mixing ratio time-profile from three days of observations (3, 4 and 10 August) when BrO was observed from dawn onwards. The sunrise time at Mace Head for this time of the year was around 04:50 UT, with a 43 min twilight period defined as the period when the SZA is between 96° and 90°. Twilight needs to be considered because, as we show below, some bromine atom precursors are very photolabile. After the BrO pulse, a rapid decrease in its mixing ratio was observed, followed by a partial recovery before noon. Figure 9 indicates that a second small maximum may also be present in the late afternoon before sunset, after which BrO decreased below the detection limit of the DOAS instrument (~1 ppt).

It is unlikely that the post-dawn BrO pulse results from the photolysis of organic bromine species, because of their long photolytic lifetimes in the lower atmosphere (Carpenter et al., 1999). One relatively short-lived alkyl bromide is CH_2IBr; however, its photolytic lifetime is still about 1 h, and its mixing ratio in the MBL at Mace Head is ~0.1 ppt (Carpenter et al., 1999). In any case, halocarbon emissions at Mace Head are driven by tidal height (Carpenter et al., 1999), and there is no correlation with tidal height evident in the BrO measurements.

Hence, the most likely BrO precursors are inorganic bromine species such as Br_2, IBr, BrCl and $BrNO_2$, which have built up after heterogeneous processing through sea-salt aerosol during the preceding night. At sunrise they are rapidly photolysed to yield Br atoms which react with O_3 to form BrO. An interesting problem is to determine which

of these potential precursors is the main contributor to the post-sunrise BrO pulse. In Fig. 10a the absorption cross-sections of these four bromine precursors are plotted against wavelength, using data from Atkinson et al. (2000). It can be seen that IBr has the largest cross-section, peaking around 500 nm and extending throughout the visible region of the spectrum. IBr will therefore photolyse most readily around dawn. In contrast, $BrNO_2$ has an absorption cross-section nearly an order of magnitude smaller, peaking at 300 nm. The rates of photodissociation (J) of $BrNO_2$, Br_2, IBr and BrCl are shown in Fig. 10b as a function of time of day, for the location of Mace Head in early August. The J values are calculated, assuming a quantum yield of unity, by an explicit two-stream radiation code (Thompson, 1984), where the incident actinic flux (photons cm^{-2} s^{-1} nm^{-1}) at the Earth's surface is obtained after attenuation through 50 atmospheric layers of 1 km height. Immediately after sunrise, J_{IBr} is twice as fast as J_{Br_2} and up to an order of magnitude faster than J_{BrNO_2}. Indeed, if $BrNO_2$ (and to a lesser extent BrCl) were the major sources of atomic Br, then the BrO pulse would be delayed in appearance and also less sharp.

Laboratory studies of the uptake of N_2O_5 on a saline surface mimicking sea-salt aerosols, which are ~660 times more concentrated in Cl^- than Br^-, have been reported by Behnke et al. (1994):

$$N_2O_{5(g)} \rightarrow N_2O_{5(aq)} \quad (2)$$

$$N_2O_{5(aq)} + X^- \rightarrow NO_3^- + XNO_2 \quad (3)$$

where X is Cl or Br. The authors found that ~10% of the released product was $BrNO_2$, with 73% $ClNO_2$ and 17% Br_2. Assuming this product yield for $BrNO_2$ and using the NO_3 chemistry model described in Sect. 3.1, we calculate that for clean marine conditions ($[NO_3]$ and $[N_2O_5]$ ~3 ppt) the cycling through sea-salt aerosol during the night would yield a BrNO2 mixing ratio of ≤0.2 ppt before sunrise.

When photolysis ceases after sunset, the uptake of HOBr or $BrNO_3$ on sea-salt aerosol will be their major removal pathways. These species will be rapidly recycled

ACPD
5, 9731–9767, 2005

through heterogeneous reactions to gas-phase Br_2 and BrCl, depending on the availability of Cl^- and Br^- (Finlayson-Pitts, 2003):

$$HOBr + Cl^- + H^+ \rightarrow BrCl + H_2O \quad (4)$$

$$BrCl + Br^- \leftrightarrow Br_2Cl^- \quad (5)$$

$$Br_2Cl^- \leftrightarrow Br_2 + Cl^- \quad (6)$$

If the Br^- concentration is sufficient (i.e., in freshly generated sea-salt aerosol), BrCl will be converted into Br_2 via Reactions (5) and (6). In aged sea-salt aerosol that is depleted in Br^-, BrCl becomes the major product (Fickert et al., 1999; Liu and Margerum, 2001; Adams et al., 2002).

Although the I^- content in sea-salt is negligible compared to Cl^- and Br^-, a similar mechanism to Reaction (4) can proceed following uptake of species such as HOI and INO_3, leading to the release of ICl and IBr to the gas phase (Vogt et al., 1999; McFiggans et al., 2000). From laboratory experiments, the main di-halogen gas-phase product is IBr from freshly generated NaCl/NaBr surfaces with sufficient Br^- content. Release of ICl was only observed after depletion of Br^- (Holmes et al., 2001). The corresponding Henry's law constants (mol l^{-1} atm^{-1}) for the different species are: $BrNO_2$ 0.3, Br_2 1.8, BrCl 0.59 (Frenzel et al., 1998) and 110 and 24 for ICl and IBr, respectively (Wagman et al., 1982).

Considering the above photodissociation rates and the mechanisms for recycling halogens through sea salt, it seems that Br_2 and IBr should be the primary sources of the large post-sunrise BrO pulses observed at Mace Head. However, from our DOAS observations there is no evidence of a post-sunrise pulse of IO (apart from when low tide coincides with sunrise). Putting this together with the fact that the solubility constant of IBr is an order of magnitude greater than that of Br_2, we infer that Br_2 is probably the dominant source of Br at sunrise in this location.

ACPD
5, 9731–9767, 2005

3.6. Modelling the diurnal behaviour of BrO

We now describe a model of bromine chemistry, containing the gas-phase reactions, photochemistry, and heterogeneous uptake processes listed in Table 1. The photolysis rates were calculated off-line using a two-stream radiation scheme. The model is solved using a variable step-size fourth-order Runge-Kutta integrator (Press et al., 1986). All bromine-containing species and O_3 are allowed to vary. The mixing ratios of the following species are held constant at values typical of clean MBL conditions: [NO_2]=30 ppt; [NO]=5 and 0 ppt at day- and nighttime, respectively; [DMS]=100 ppt; [CH_2IBr]=0.1 ppt. The mixing ratios of OH and HO_2 are constrained in the model to follow the diurnal profiles of these radicals measured during NAMBLEX, with noon maxima of 0.1 and 5 ppt, respectively (Bloss et al., 2005).

The heterogeneous reaction of HOBr with sea salt and subsequent liberation of Br_2 and BrCl to the gas phase has been observed to occur rapidly (Abbatt and Waschewsky, 1998; Fickert et al., 1999; Adams et al., 2002). These experiments were conducted on surfaces with a Cl^-/Br^- ratio of ~660. Considering the aqueous phase reaction rates and equilibrium constants for Reactions (4–6) (Liu and Margerum, 2001; Finlayson-Pitts, 2003), a simple calculation shows that it would take a few minutes for HOBr, once taken up on a sea-salt aerosol surface, to be released as Br_2 and, to a lesser extent BrCl, depending upon the Br^- content and acidity of the aerosol (Fickert et al., 1999). Hence, the rate-limiting step of this heterogeneous process will be the uptake of HOBr on the aerosol surface. In the model runs shown here we consider the uptake of HOBr to generate 75% Br_2 and 25% BrCl.

Likewise, aqueous phase reactions involving $BrNO_3$ could also lead to the release of Br_2 and BrCl via hydrolysis or reaction with Cl^- and Br^- (Sander et al., 1999):

$$BrNO_3 + H_2O \rightarrow HOBr + HNO_3 \quad (7)$$

$$BrNO_3 + Cl^- \rightarrow BrCl + NO_3^- \quad (8)$$

$$BrNO_3 + Br^- \rightarrow Br_2 + NO_3^- \quad (9)$$

ACPD
5, 9731–9767, 2005

Reaction of $BrNO_3$ on aerosol surfaces via Reactions (8) and (9) can proceed without aerosol acidity, and hence allow halogen activation on alkaline aerosols (Sander et al., 1999). Figure 11 shows the result of a model simulation for clean marine conditions, where the sea-salt surface area is set to 10^{-7} cm^2 cm^{-3}. The model is initialised with Br_2 and BrCl mixing ratios of 4.5 and 1.5 ppt, respectively. A rapid pulse of BrO up to 4.5 ppt is generated as soon as photolysis starts. In order to match the observed pulse of BrO (Fig. 9) the rate of post-sunrise Br atom production needed is $\sim 8 \times 10^3$ molecule cm^{-3} s^{-1}. As Br_2 and BrCl are photolysed and their mixing ratio rapidly decreases, BrO reaches a minimum followed by a slow recovery throughout the day leading to a second maximum in the late afternoon. BrO then disappears as photolysis ceases after sunset. Similar diurnal behaviour has been predicted in previous studies (Sander et al., 1999; Glasow et al., 2002). The modelled BrO time-profile in Fig. 11 is comparable to that observed (Fig. 9), with midday/afternoon mixing ratios around 1.5–2.5 ppt (Saiz-Lopez et al., 2004). Note that this model does not incorporate BrO mixing within the boundary layer. The BrO increase towards the late afternoon is due to the recycling of HOBr and $BrNO_3$ through sea-salt aerosol.

After sunset, large amounts of $BrNO_3$ build up as photolysis ceases, and this becomes the major bromine species. In this model run $BrNO_3$ has a loss rate due to uptake on aerosols of $\sim 1 \times 10^{-5}$ s^{-1} if γ=0.02 (note that the uptake of $BrNO_3$ on deliquesced sea salt aerosols does not appear to have been measured). The daytime average photolysis rate of $BrNO_3$ is $\sim 8.5 \times 10^{-4}$ s^{-1}, so this will probably be the dominant loss process, competing with thermal decomposition which has a measured rate of 9×10^{-6} s^{-1} at 290 K (Orlando and Tyndall, 1996). The $BrNO_3$ time-profile in Fig. 11 exhibits two distinct peaks: after the sunrise BrO pulse, and in the early evening when photolysis slows down. The $BrNO_3$ minimum around noon is caused by photolysis, which is sharply peaked to noon because the molecule absorbs almost entirely in the near-UV. After sunset the remaining $BrNO_3$ is slowly taken up on aerosols, and this is most likely the major route to the overnight build-up of gas-phase Br_2.

HOBr follows the diurnal behaviour of HO_2, with a maximum at midday. HOBr re-

moval during daytime is dominated by photodissociation, as J_{HOBr} is about 40 times greater than heterogeneous loss to form Br_2 and BrCl. Here a γ of 0.05 for HOBr is used, in accord with a lower limit of $\gamma > 10^{-2}$ measured on aqueous salt solutions (Fickert et al., 1999; Adams et al., 2002). Note that Abbatt and Waschewsky (1998) reported $\gamma > 0.2$ for deliquescent NaCl aerosols within an acidity pH range 0.3–7. HOBr uptake and production of gas-phase bromine-containing is dependant on aerosol acidity, and decreases with decreasing acidity (Fickert et al., 1999). Here we are assuming a scenario of freshly generated sea-salt aerosols with pH = 8, the same as ocean water (Glasow et al., 2002, and references therein). It must be noted that the progressive acidification of aerosols by uptake of species such as HNO_3, H_2SO_4 and SO_2 is not treated in the model. Considering an average volume concentration of aerosol (diameter = 0.3–47 μm) measured during NAMBLEX of 400 μm^3 cm^{-3} (G. McFiggans, personal communication, 2005) and a Br^- content in sea salt of 8×10^{-3} mol l^{-1} we calculate a Br^- depletion from sea-salt of 22% over the 1-day model run.

After sunset, the main sink for HOBr is heterogeneous uptake, contributing to the nighttime production of gas-phase bromine atom precursors: Fig. 11 shows the Br_2 build up once photolysis ceases leading to a maximum before sunrise, which will be responsible of the second post-dawn BrO pulse. Note that O_3 is depleted through the day at a rate of approximately 0.06 ppb h^{-1}, mainly through the cycle involving BrO+HO_2. Of course, this is a zero-dimensional model and does not include mixing with O_3-rich air from aloft.

4. Conclusions

The techniques of long-path DOAS and zenith sky spectroscopy have been employed to acquire a comprehensive set of measurements of I_2, IO, OIO, BrO and NO_3 in a coastal mid-latitude location. The time series of the different species over a month of observations are summarised in this paper. The observed daytime mixing ratios of the halogen oxides will affect a number of atmospheric processes such as ozone de-

ACPD
5, 9731–9767, 2005

pletion, DMS oxidation capacity, new particle formation and regulation of the HO_2/OH and NO_2/NO ratios. Model simulations show that the reaction between NO_3 and I_2 probably accounts for the significant nighttime levels of iodine oxides found at Mace Head. The observed pulses of BrO at sunrise, and subsequent diurnal behaviour of the radical, are explained with a model that incorporates the processing of the major daytime bromine reservoirs, $BrNO_3$ and HOBr, through sea-salt aerosol. However, the NAMBLEX data-set on BrO is quite small and more field observations are needed in order to establish this diurnal behaviour. Finally, the combination of boundary layer and vertical profile measurements of NO_3 indicates that this radical often exists at higher concentration in the upper MBL and lower free troposphere, probably reflecting the efficient removal of NO_3 by DMS close to the ocean surface.

Acknowledgements. This work was supported by the Natural Environment Research Council of the UK. The authors wish to thank D. Heard (University of Leeds) for leading the NAMBLEX campaign and B. Allan for helpful discussions.

References

Abbatt, J. P. D. and Waschewsky, G. C. G.: Heterogeneous interactions of HOBr, HNO_3, O_3 and NO_2 with deliquescent NaCl aerosols at room temperature, J. Phys. Chem. A, 102, 3719–3725, 1998. 9746, 9748

Adams, J. W., Holmes, N. S., and Crowley, J. N.: Uptake and reaction of HOBr on frozen and dry NaCl/NaBr surfaces between 253 and 233 K, Atmos. Chem. Phys., 2, 79–91, 2002, SRef-ID: 1680-7324/acp/2002-2-79. 9745, 9746, 9748, 9756

Alicke, B., Hebestreit, K., Stutz, J., and Platt, U.: Iodine oxide in the marine boundary layer, Nature, 397, 572–573, 1999. 9733, 9740

Allan, B. J. and Plane, J. M. C.: A study of the recombination of IO and NO_2 and the stability of INO_3: implications for the atmospheric chemistry of iodine, J. Phys. Chem. A, 106, 8634–8641, 2002b. 9741

Allan, B. J., Carslaw, N., Coe, H., Burgess, R. A., and Plane, J. M. C.: Observations of the nitrate radical in the marine boundary layer, J. Atmos. Chem., 33, 129–154, 1999. 9736

Allan, B. J., McFiggans, G., Plane, J. M. C., and Coe, H.: Observations of iodine monoxide in the remote marine boundary layer, J. Geophys. Res.-Atmos, 105, 14 363–14 369, 2000a. 9733, 9740

Allan, B. J., McFiggans, G., Plane, J. M. C., and McFadyen, G. G.: The nitrate radical in the remote marine boundary layer, J. Geophys. Res.-Atmos, 105, 24 191–24 204, 2000b. 9734, 9736, 9737

Allan, B. J., Plane, J. M. C., and McFiggans, G.: Observations of OIO in the remote marine boundary layer, Geophys. Res. Lett., 28, 1945–1948, 2001. 9733, 9740

Allan, B. J., Plane, J. M. C., Coe, H., and Shillito, J. A.: Observations of NO_3 concentration profiles in the troposphere, J. Geophys. Res., 107, art. no. 4588, doi:10.1029/2002JD002112, 2002a. 9734, 9735, 9737, 9738

Ashworth, S. H., Allan, B. J., and Plane, J. M. C.: High resolution spectroscopy of the OIO radical: Implications for the ozone-depleting potential of iodine, Geophys. Res. Lett., 29, art. no. 1456, doi:10.1029/2001GL013851, 2002. 9740

Atkinson, R., Baulch, D. L., Cox, R. A., Crowley, J. N., Hampson Jr., R. F., Hynes, R. G., Jenkin, M. E., Kerr, J. A., Rossi, M. J., and Troe, J.: Summary of evaluated kinetic and photochemical data for atmospheric chemistry, IUPAC, J. Phys. Chem. Ref. Data, 29, 167–266, http://www.iupac-kinetic.ch.cam.ac.uk/, 2000. 9742, 9744, 9756

Ayers, G. P., Gillet, R. W., Cainey, J. M., and Dick, A. L.: Chloride and bromide loss froma sea-salt particles in Southern Ocean air, J. Atmos. Chem., 33, 299–319, 1999. 9733

Barrie, L. A., Bottenheim, J. W., Schnell, R. C., Crutzen, P. J., and Rasmussen, R. A.: Ozone destruction and photochemical-reactions at polar sunrise in the lower Arctic atmosphere, Nature, 334, 138–141, 1988. 9732

Behnke, W., Scheer, V., and Zetzsch, C.: Production of $BrNO_2$, Br_2 and $ClNO_2$ from the reaction between sea spray aerosol and N_2O_5, J. Aero. Sci., 25, S277–S278, 1994. 9733, 9744

Behnke, W., George, C., Scheer, V., and Zetzsch, C.: Production and decay of $ClNO_2$ from the reaction of gaseous N_2O_5 with NaCl solution: bulk and aerosol experiments, J. Geophys. Res.-Atmos, 102, 3795–3804, 1997. 9737

Bloss, W. J., Lee, J. D., Johnson, G. P., Sommariva, R., Heard, D. E., Saiz-Lopez, A., Plane, J. M. C., McFiggans, G., Coe, H., Flynn, M., Williams, P., Rickard, A. R., and Fleming, Z.: Impact of halogen monoxide chemistry upon boundary layer OH and HO_2 concentrations at a coastal site, Geophys. Res. Lett., 32, art. no. L06814, doi:10.1029/2004GL022084, 2005. 9733, 9746

Brown, S. S., Stark, H., Ryerson, T. B., Williams, E. J., Nicks, D. K., Trainer, M., Fehsenfeld, F. C., and Ravishankara, A. R.: Nitrogen oxides in the nocturnal boundary layer: Simultaneous in situ measurements of NO_3, N_2O_5, NO_2, NO, O_3, J. Geophys. Res.-Atmos, 108, art. no. 4299, doi:10.1029/2002JD002917, 2003. 9734

Brown, S. S., Dibb, J. E., Stark, H., Aldener, M., Vozella, M., Whitlow, S., Williams, E. J., Lerner, B. M., Jakoubek, R., Middlebrook, A. M., DeGouw, J. A., Warneke, C., Goldan, P. D., Kuster, W. C., Angevine, W. M., Sueper, D. T., Quinn, P. K., Bates, T. S., Meagher, J. F., Fehsenfeld, F. C., and Ravishankara, A. R.: Nighttime removal of NO_x in the summer marine boundary layer, Geophys. Res. Lett., 31, art. no. L07108, doi:10.1029/2004GL019412, 2004. 9734, 9736

Butkovskaya, N. I. and LeBras, G.: Mechanism of the NO_3 + DMS reaction by discharge flow mass- spectrometry, J. Phys. Chem. A, 98, 2582–2591, 1994. 9734

Carpenter, L. J., Sturges, W. T., Penkett, S. A., Liss, P. S., Alicke, B., Hebestreit, K., and Platt, U.: Short-lived alkyl iodides and bromides at Mace Head, Ireland: Links to biogenic sources and halogen oxide production, J. Geophys. Res.-Atmos, 104, 1679–1689, 1999. 9733, 9743

Chambers, R. M., Heard, A. C., and Wayne, R. P.: Inorganic gas-phase reactions of the nitrate radical – I_2+NO_3 and I+NO_3, J. Phys. Chem. A, 96, 3321–3331, 1992. 9733, 9741

Coe, H., Allan, B. J., and Plane, J. M. C.: Retrieval of vertical profiles of NO_3 from zenith sky measurements using an optimal estimation method, J. Geophys. Res.-Atmos, 107, art. no. 4587, doi:10.1029/2002JD002111, 2002. 9737, 9738

Davis, D. J., Crawford, J., Liu, S., McKeen, S., Bandy, A., Thorton, D., Rowland, F., and Blake, D.: Potential impact of iodine on tropospheric levels of Ozone and other critical oxidants, J. Geophys. Res.-Atmos, 101, 2135–2147, 1996. 9733

Deiber, G., George, C., Calve, S. L., Schweitzer, F., and Mirabel, P.: Uptake study of $ClNO_2$ and $BrNO_2$ by halide containing droplets, Atmos. Chem. Phys., 4, 1291–1299, 2004, SRef-ID: 1680-7324/acp/2004-4-1291. 9756

Farman, J. C., Gardiner, B. G., and Shanklin, J. D.: Large losses of total ozone in Antarctica reveal seasonal ClO_x/NO_x interaction, Nature, 315, 207–210, 1985. 9732

Fickert, S., Adams, J. W., and Crowley, J. N.: Activation of Br_2 and BrCl via uptake of HOBr onto aqueous salt solutions, J. Geophys. Res.-Atmos, 104, 23 719–23 727, 1999. 9745, 9746, 9748, 9756

Finlayson-Pitts, B. J.: The tropospheric chemistry of sea salt: a molecular-level view of the chemistry of NaCl and NaBr, Chem. Rev., 103, 4801–4822, 2003. 9745, 9746

Finlayson-Pitts, B. J., Livingston, F. E., and Berko, H. N.: Ozone destruction and bromine photochemistry at ground-level in the Arctic spring, Nature, 343, 622–625, 1990. 9732
Frenzel, A., Scheer, V., Sikorski, R., George, C., Behnke, W., and Zetzsch, C.: Heterogeneous interconversion reactions of $BrNO_2$, $ClNO_2$, Br_2 and Cl_2, J. Phys. Chem. A, 102, 1329–1337, 1998. 9745
Gabriel, R., von Glasow, R., Sander, R., Andreae, M. O., and Crutzen, P. J.: Bromide content of sea-salt aerosols collected over the Indian Ocean during INDOEX 1999, J. Geophys. Res.-Atmos, 107, 8032, doi:10.1029/2001JD001133, 2002. 9733
Garland, J. A. and Curtis, H.: Emission of iodine from the sea surface in the presence of ozone, J. Geophys. Res.-Atmos, 86, 3183–3186, 1981. 9739
Glasow, R. V. and Crutzen, P. J.: Model study of multiphase DMS oxidation with a focus on halogens, Atmos. Chem. Phys., 4, 589–608, 2004, SRef-ID: 1680-7324/acp/2004-4-589. 9733
Glasow, R. V., Sander, R., Bott, A., and Crutzen, P. J.: Modelling halogen chemistry in the marine boundary layer 1. Cloud-free MBL, J. Geophys. Res.-Atmos, 107, 4341, doi:10.1029/2001JD000942, 2002. 9747, 9748
Harwood, M. H., Burkholder, J. B., Hunter, M., Fox, R. W., and Ravishankara, A. R.: Absorption cross sections and self-reaction kinetics of the IO radical, J. Phys. Chem. A, 101, 853–863, 1997. 9735
Hausmann, M. and Platt, U.: Spectroscopic measurement of bromine oxide and ozone in the high Arctic during Polar Sunrise Experiment 1992, J. Geophys. Res.-Atmos, 99, 25 399–25 413, 1994. 9732
Heintz, F., Platt, U., Flentje, H., and Dubois, R.: Long-term observation of nitrate radicals at the Tor station, Kap Arkona (Rugen), J. Geophys. Res.-Atmos, 101, 22 891–22 910, 1996. 9734, 9736
Holmes, N. S., Adams, J. W., and Crowley, J. N.: Uptake and reaction of HOI and $IONO_2$ on frozen and dry NaCl/NaBr surfaces and H_2SO_4, Phys. Chem. Chem. Phys., 3, 1679–1687, 2001. 9745
Honninger, G. and Platt, U.: Observations of BrO and its vertical distribution during surface ozone depletion at Alert, Atmos. Environ., 36, 2481–2489, 2002. 9732
Jenkin, M. E., Cox, R. A., and Candeland, D. E.: Photochemical aspects of tropospheric iodine behavior, J. Atmos. Chem., 2, 359–375, 1985. 9733
Kupper, F. C., Schweigert, N., Gall, E. A., Legendre, J. M., Vilter, H., and Kloareg, B.: Iodine

uptake in Laminariales involves extracellular, haloperoxidase-mediated oxidation of iodide, Planta, 207, 163–171, 1998. 9739
Leser, H., Honninger, G., and Platt, U.: MAX-DOAS measurements of BrO and NO_2 in the marine boundary layer, Geophys. Res. Lett., 30, doi:10.1029/2002GL015811, 2003. 9733
Liu, Q. and Margerum, D. W.: Equilibrium and kinetics of bromine chloride hydrolysis, Environ. Sci. Tech., 35, 1127–1133, 2001. 9745, 9746
McConnell, J. C., Henderson, G. S., Barrie, L., Bottenheim, J., Niki, H., Langford, C. H., and Templeton, E. M. J.: Photochemical bromine production implicated in Arctic boundary-layer ozone depletion, Nature, 355, 150–152, 1992. 9732
McFiggans, G., Plane, J. M. C., Allan, B. J., Carpenter, L. J., Coe, H., and O'Dowd, C.: A modeling study of iodine chemistry in the marine boundary layer, J. Geophys. Res.-Atmos, 105, 14 371–14 385, 2000. 9733, 9741, 9745
McFiggans, G., Coe, H., Burgess, R., Allan, J., Cubison, M., Alfarra, M. R., Saunders, R., Saiz-Lopez, A., Plane, J. M. C., Wevill, D. J., Carpenter, L. J., Rickard, A. R., and Monks, P. S.: Direct evidence for coastal iodine particles from Laminaria macroalgae - linkage to emissions of molecular iodine, Atmos. Chem. Phys., 4, 701–713, 2004, SRef-ID: 1680-7324/acp/2004-4-701. 9734, 9739
Misra, A. and Marshall, P.: Computational investigations of iodine oxides, J. Phys. Chem. A, 102, 9056–9060, 1998. 9742
Molina, M. J. and Rowland, F. S.: Stratospheric sink for chlorofluoromethanes – chlorine atom-catalysed destruction of ozone, Nature, 249, 810–812, 1974. 9732
O'Dowd, C. D., Jimenez, J. L., Bahreini, R., Flagan, R. C., Seinfeld, J. H., Hameri, K., Pirjola, L., Kulmala, M., Jennings, S. G., and Hoffmann, T.: Marine aerosol formation from biogenic iodine emissions, Nature, 417, 632–636, 2002. 9734
Orlando, J. J. and Tyndall, G. S.: Rate coefficients for the thermal decomposition of $BrONO_2$ and the heat of formation of $BrONO_2$, J. Phys. Chem. A, 100, 19 398–19 405, 1996. 9747, 9756
Plane, J. M. C. and Saiz-Lopez, A.: UV-visible Differential Optical Absorption Spectroscopy (DOAS), in: Analytical Techniques for Atmospheric Measurement; edited by: Heard, D. E., Blackwell Publishing, Oxford, in press, 2005. 9735
Platt, U., Perner, D., Harris, G. W., Winer, A. M., and Pitts, J. N.: Detection of NO_3 in the polluted troposphere by differential optical absorption, Geophys. Res. Lett., 7, 89–92, 1980. 9734
Platt, U., LeBras, G., Poulet, G., Burrows, J. P., and Moortgat, G.: Peroxy radicals from night-

time reaction of NO_3 with organic compounds, Nature, 348, 147–149, 1990. 9734
Press, W. H., Flannery, B. P., Teukolsky, S. A., and Vetterling, W. T.: Numerical recipes: The art of scientific computing, Cambridge University Press, Cambridge, 1986. 9746
Rodgers, C. D.: Retrieval of atmospheric temperature and composition from remote measurements of thermal-radiation, Rev. Geophys., 14, 609–624, 1976. 9738
Rodgers, C. D.: Characterization and error analysis of profiles retrieved from remote sounding measurements, J. Geophys. Res.-Atmos, 95, 5587–5595, 1990. 9738
Saiz-Lopez, A. and Plane, J. M. C.: Novel iodine chemistry in the marine boundary layer, Geophys. Res. Lett., 31, art. no. L04112, doi:10.1029/2003GL019215, 2004. 9733, 9739, 9740, 9741, 9742
Saiz-Lopez, A., Plane, J. M. C., and Shillito, J. A.: Bromine oxide in the mid-latitude marine boundary layer, Geophys. Res. Lett., 31, art. no. L03111, doi:10.1029/2003GL018956, 2004a. 9733, 9743
Saiz-Lopez, A., Saunders, R. W., Joseph, M., and Plane, J. M. C.: Absolute absorption cross-section and photolysis rate of I_2, Atmos. Chem. Phys., 4, 1443–1450, 2004b, SRef-ID: 1680-7324/acp/2004-4-1443. 9735
Saiz-Lopez, A., Plane, J. M. C., McFiggans, G., Williams, P. I., Ball, S. M., Bitter, M., Jones, R. L., Hongwei, C., and Hoffmann, T.: Modelling molecular iodine emissions in a coastal marine environment: the link to new particle formation, Atmos. Chem. Phys. Discuss., 5, 5405–5439, 2005, SRef-ID: 1680-7375/acpd/2005-5-5405. 9734, 9739, 9740, 9741, 9742, 9743
Sander, R., Rudich, Y., von Glasow, R., and Crutzen, P. J.: The role of $BrNO_3$ in marine tropospheric chemistry: A model study, Geophys. Res. Lett., 26, 2857–2860, 1999. 9746, 9747
Sander, S. P., Friedl, R. R., Golden, D. M., Kurylo, M. J., Huie, R. E., Orkin, V. L., Moortgat, G. K., Ravishankara, A. R., Kolb, C. E., Molina, M., and Finlayson-Pitts, B. J.: Chemical kinetics and photochemical data for use in stratospheric modeling: Evaluation 14, Tech. rep., Jet Propulsion Laboratory, Pasadena, California, USA, http://jpldataeval.jpl.nasa.gov/, 2003. 9736, 9756
Schweitzer, F., Mirabel, P., and George, C.: Multiphase chemistry of N_2O_5, $ClNO_2$, $BrNO_2$, J. Phys. Chem. A, 102, 3942–3952, 1998. 9756
Smith, J. P. and Solomon, S.: Atmospheric NO_3. 3. Sunrise disappearance and the stratospheric profile, J. Geophys. Res.-Atmos, 95, 13 819–13 827, 1990. 9737

Smith, J. P., Solomon, S., Sanders, R. W., Miller, H. L., Perliski, L. M., Keys, J. G., and Schmeltekopf, A. L.: Atmospheric NO_3. 4. Vertical profiles at middle and polar latitudes at sunrise, J. Geophys. Res.-Atmos, 98, 8983–8989, 1993. 9737

Thompson, A. M.: The effect of clouds on photolysis rates and ozone formation in the unpolluted troposphere, J. Geophys. Res.-Atmos, 89, 1341–1349, 1984. 9744

Truesdale, V. W., Luther, G. W., and Canosamas, C.: Molecular iodine reduction in seawater – an improved rate equation considering organic compounds, Mar. Chem., 48, 2, 143–150, 1995. 9739

Vogt, R., Crutzen, P. J., and Sander, R.: A mechanism for halogen release from sea-salt aerosol in the remote marine boundary layer, Nature, 383, 327–330, 1996. 9733

Vogt, R., Sander, R., Glasow, R. V., and Crutzen, P. J.: Iodine chemistry and its role in halogen activation and ozone loss in the marine boundary layer: A model study, J. Atmos. Chem., 32, 375–395, 1999. 9745

Vrekoussis, M., Kanakidou, M., Mihalopoulos, N., Crutzen, P. J., Lelieveld, J., Perner, D., Berresheim, H., and Baboukas, E.: Role of the NO_3 radicals in oxidation processes in the eastern Mediterranean troposphere during the MINOS campaign, Atmos. Chem. Phys., 4, 169–182, 2004,
SRef-ID: 1680-7324/acp/2004-4-169. 9736

Wagman, D. D., Evans, W. H., Parker, V. B., Schumm, R. H., Halow, I., Bailey, S. M., Churney, K. L., and Nuttall, R. L.: The NBS tables of chemical thermodynamic properties; Selected values for inorganic and C_1 and C_2 organic substances in SI units, J. Phys. Chem. Ref. Data, 11, suppl. 2, 1982. 9745

Wahner, A., Ravishankara, A. R., Sander, S. P., and Friedl, R. R.: Absorption cross-section of BrO between 312 and 385 nm at 298 and 223 K, Chem. Phys. Lett., 152, 507–512, 1988. 9735

Wofsy, S. C., McElroy, M. B., and Yung, Y. L.: The chemistry of atmospheric bromine, Geophys. Res. Lett., 2, 215–218, 1975. 9732

Yokelson, R. J., Burkholder, J. B., Fox, R. W., Talukdar, R. K., and Ravishankara, A. R.: Temperature-Dependence of the NO_3 absorption spectrum, J. Phys. Chem. A, 98, 13 144–13 150, 1994. 9735, 9737

Table 1. Bromine chemistry scheme used in the photochemical box model[a].

No	Reaction	Rate constant	Remarks[b]
(R1)	$Br + O_3 \rightarrow BrO + O_2$	$1.7\times10^{-11}e^{(-800/T)}$	1
(R2)	$HBr + OH \rightarrow Br + H_2O$	1.1×10^{-11}	1
(R3)	$Br + HO_2 \rightarrow HBr + O_2$	$1.5\times10^{-11}e^{(-600/T)}$	1
(R4)	$Br + NO_2 + M \rightarrow BrNO_2$	$k_o = 4.2\times10^{-31}\times(T/300)^{-2.4}$ $k_\infty = 2.7\times10^{-11}\times(T/300)^{-0}$	1
(R5)	$BrO + NO_2 + M \rightarrow BrNO_3$	$k_o = 5.2\times10^{-31}\times(T/300)^{-3.2}$ $k_\infty = 6.9\times10^{-12}\times(T/300)^{-2.9}$	1
(R6)	$BrO + HO_2 \rightarrow HOBr + O_2$	$3.4\times10^{-12}e^{(540/T)}$	1
(R7)	$BrO + NO \rightarrow Br + NO_2$	$8.8\times10^{-12}e^{(260/T)}$	1
(R8)	$BrO + CH_3SCH_3 \rightarrow CH_3SOCH_3 + Br$	$1.5\times10^{-14}e^{(850/T)}$	1
(R9)	$BrO + BrO \rightarrow 2Br + O_2$	$2.4\times10^{-12}e^{(40/T)}$	1
(R10)	$BrO + BrO \rightarrow Br_2 + O_2$	$2.8\times10^{-14}e^{(860/T)}$	1
(R11)	$BrNO_3 \rightarrow BrO + NO_2$	$2.8\times10^{13}\ e^{-(12360/T)}$	2
(R12)	$BrO + h\nu \rightarrow Br + O$	0.05	3
(R13)	$Br_2 + h\nu \rightarrow 2Br$	0.0315	3
(R14)	$IBr + h\nu \rightarrow Br + I$	0.067	3
(R15)	$BrCl + h\nu \rightarrow Br + Cl$	9.8×10^{-3}	3
(R16)	$BrNO_2 + h\nu \rightarrow Br + NO_2$	5.8×10^{-3}	3
(R17)	$BrNO_3 + h\nu \rightarrow BrO + NO_2$ (Φ=0.71) $\rightarrow Br + NO_3$ (Φ = 0.29)	1.4×10^{-3}	3
(R18)	$HOBr + h\nu \rightarrow Br + OH$	1.8×10^{-3}	3
(R19)	$CH_2IBr + h\nu \rightarrow CH_2 + Br + I$	3.8×10^{-4}	3
(R20)	Uptake coefficient of HOBr	0.05	4
(R21)	Uptake coefficient of HBr	0.03	5
(R22)	Uptake coefficient of $BrNO_3$	0.02	6

[a] Units: unimolecular reactions, s^{-1}; photolysis rate constants, s^{-1}; bimolecular reactions, cm^3 $molecule^{-1}$ s^{-1}; termolecular reactions, cm^6 $molecule^{-2}$ s^{-1}, calculated using the formalism of Sander et al. (2003), where $k=((k_o[M]/(1+k_o[M]/k_\infty))\times F_c^n)$, F_c=0.6 and $n=(1+(\log_{10}(k_o[M]/k_\infty))^2)^{-1}$.

[b] Remarks: 1, Sander et al. (2003); 2, from Orlando and Tyndall (1996), applicable for atmospheric pressure; 3, absorption cross-sections taken from Atkinson et al. (2000); 4, from Fickert et al. (1999); Adams et al. (2002); 5, from Schweitzer et al. (1998); 6, from latest IUPAC dataset 2005, estimated from Deiber et al. (2004).

ACPD
5, 9731–9767, 2005

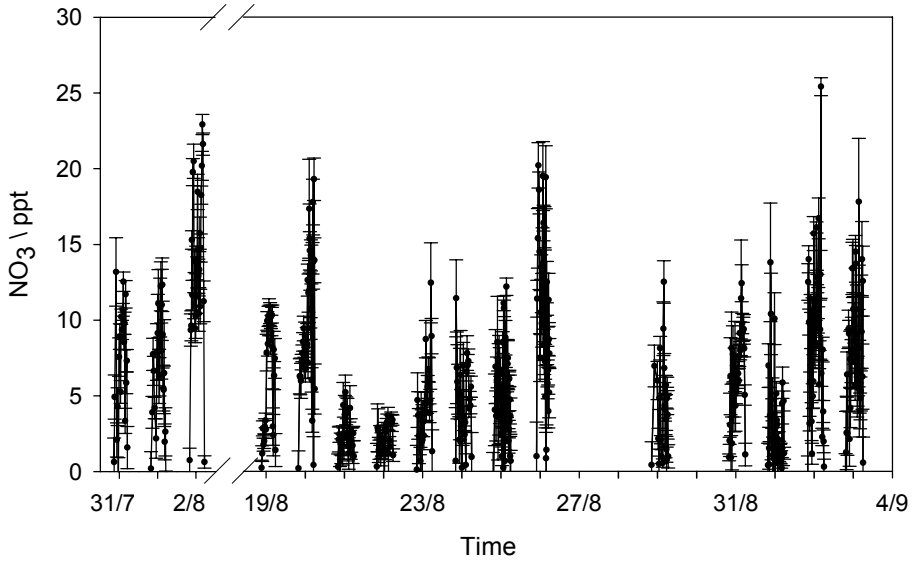

Fig. 1. NO_3 time series as measured by the LP-DOAS instrument during NAMBLEX. The mixing ratios are plotted together with the 2σ uncertainties.

ACPD
5, 9731–9767, 2005

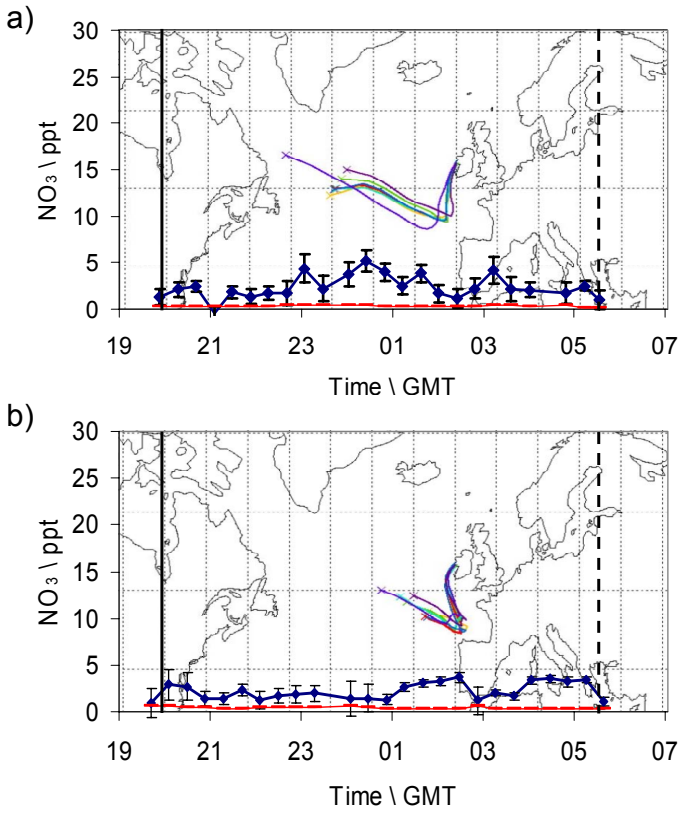

Fig. 2. Example of 5-day back trajectory in combination with a time-profile of the corresponding NO_3 mixing ratios for the westerly air masses arrival day. The solid and broken black lines correspond to dusk and dawn times, respectively, on 21 August **(a)** and 22 August **(b)**. The NO_3 mixing ratios are shown with their uncertainty and detection limit (red line). Each back trajectory shows the path of an air mass over a period of five days before its arrival at Mace Head. The arrival time is midnight and the colour coded trajectories correspond to different pressure levels.

ACPD
5, 9731–9767, 2005

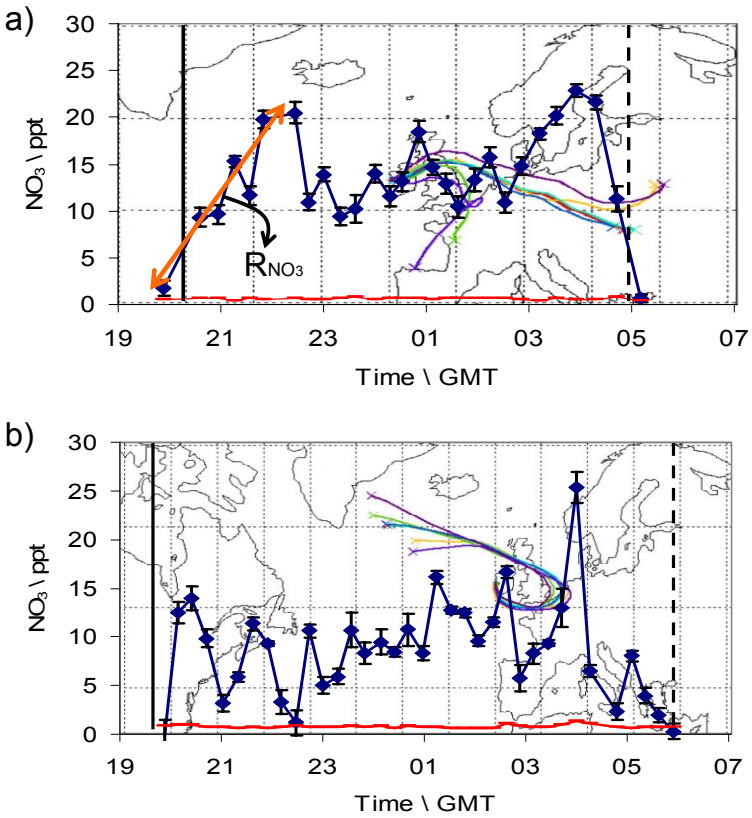

Fig. 3. Example of semi-polluted air masses and the NO_3 mixing ratio time-profiles for 1 August and 3 September. R_{NO_3} represent the rate of formation of the radical after sunset, calculated with the measured O_3 and NO_2 mixing ratios.

ACPD
5, 9731–9767, 2005

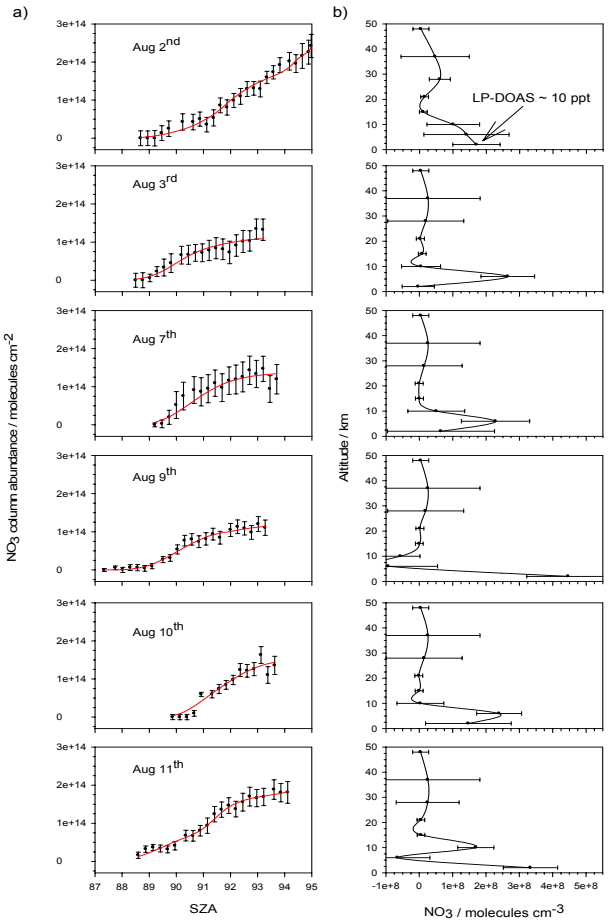

Fig. 4. (a) Zenith-sky spectroscopy measurements of the NO_3 column abundance as a function of SZA during six days of observations at Mace Head. The solid red line indicates the profile predicted by the OEM forward model. **(b)** The corresponding retrieved vertical concentration profile of NO_3.

ACPD
5, 9731–9767, 2005

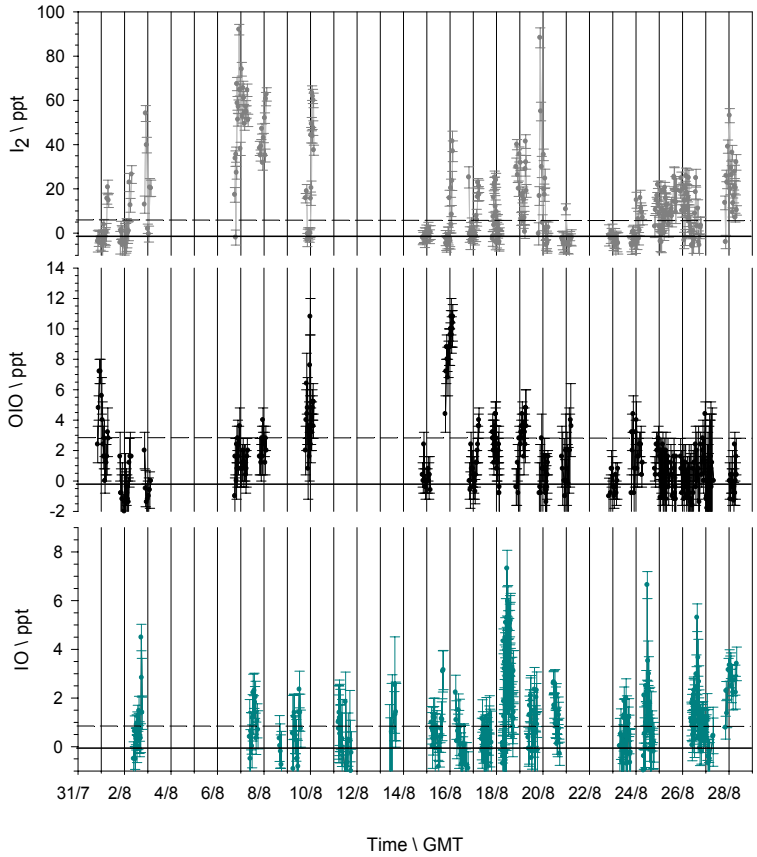

Fig. 5. Time series of I_2, IO and OIO at Mace Head during NAMBLEX. The mixing ratios are plotted with their 2σ uncertainties as well as their average detection limit through the campaign (horizontal broken line).

ACPD
5, 9731–9767, 2005

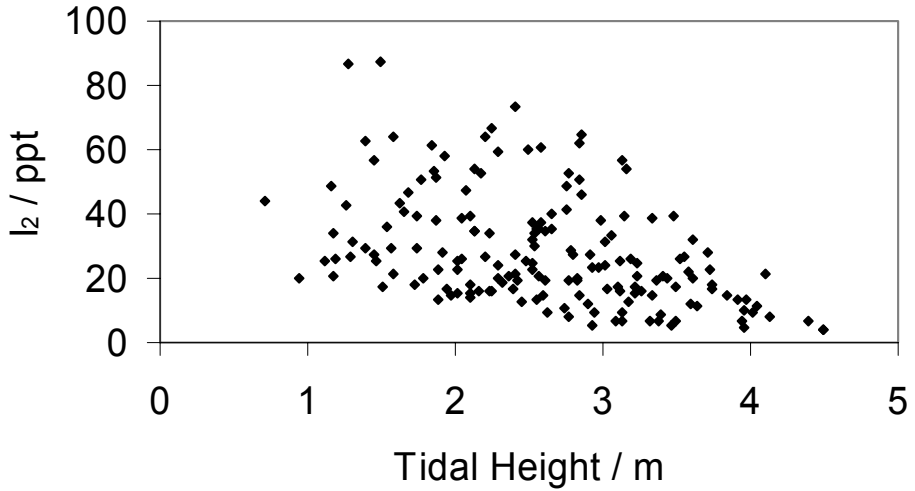

Fig. 6. Plot of I_2 mixing ratio versus tidal height at Mace Head.

ACPD
5, 9731–9767, 2005

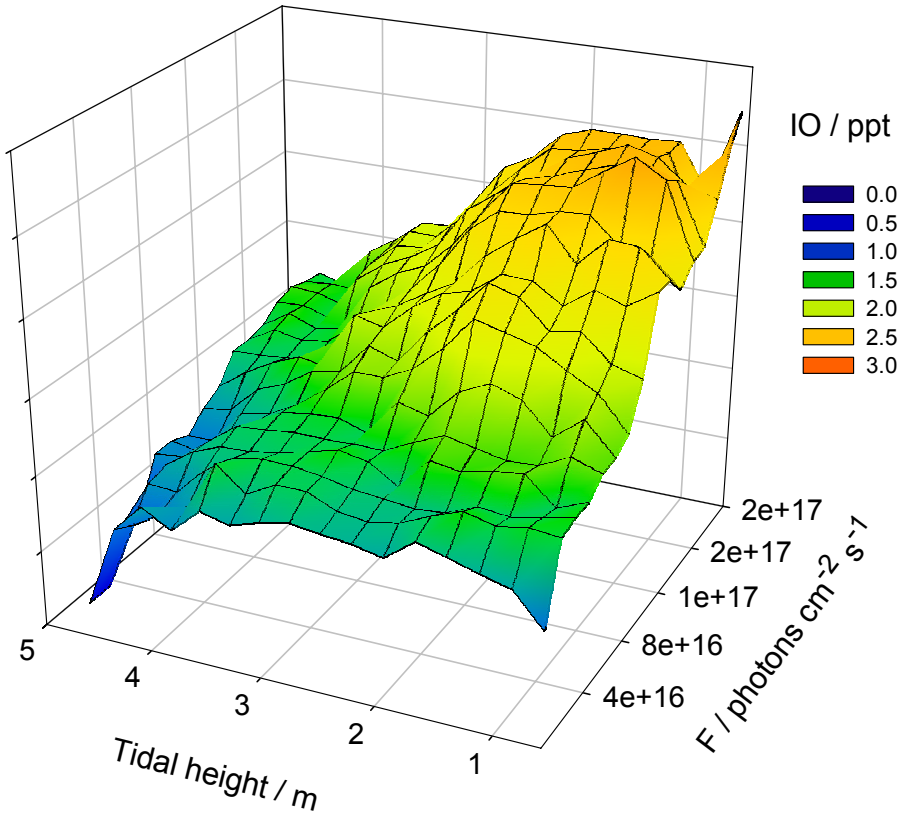

Fig. 7. Mesh plot showing the observed daytime IO as a function of tidal height and solar irradiance.

ACPD
5, 9731–9767, 2005

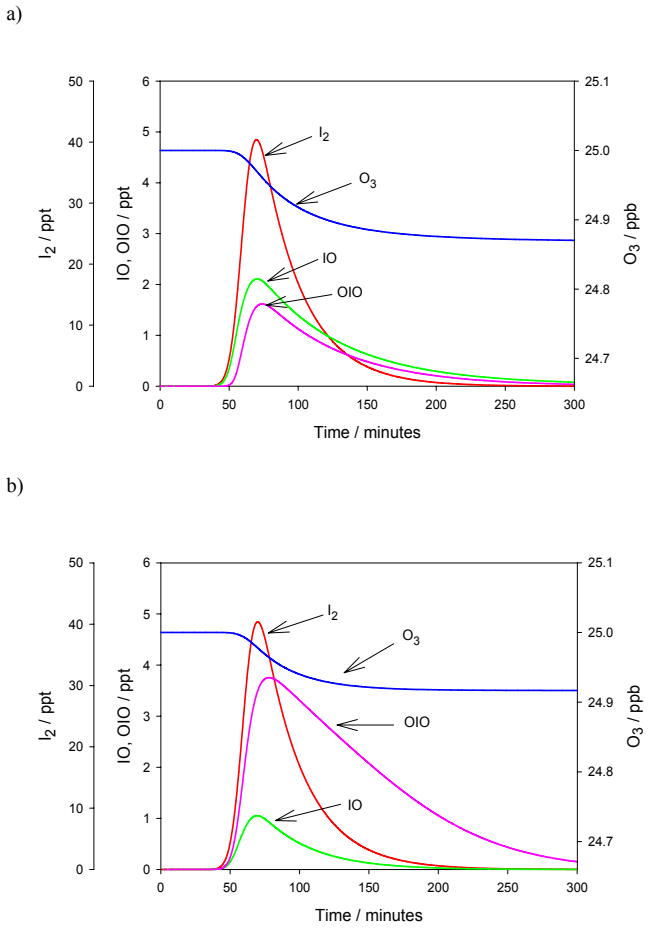

Fig. 8. (a) Nighttime run of the iodine model, with low tide 60 min after the start. **(b)** Model run with the same initial conditions as (a) but including the reaction $IO+NO_3 \rightarrow OIO+NO_2$.

ACPD
5, 9731–9767, 2005

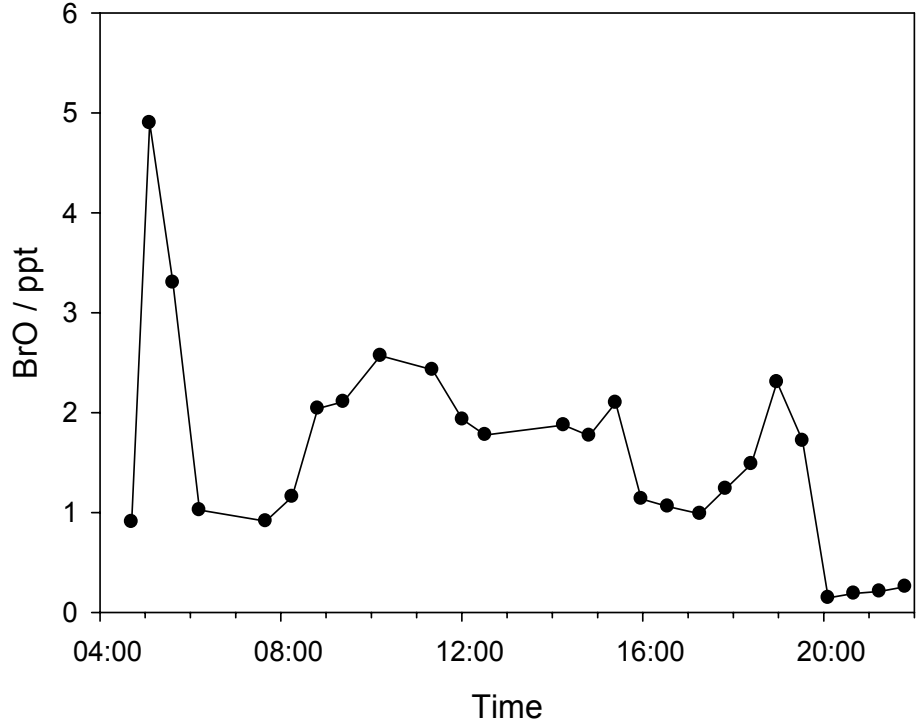

Fig. 9. Average mixing ratio time-profile of BrO during three days of NAMBLEX measurements (3, 4 and 10 August).

ACPD
5, 9731–9767, 2005

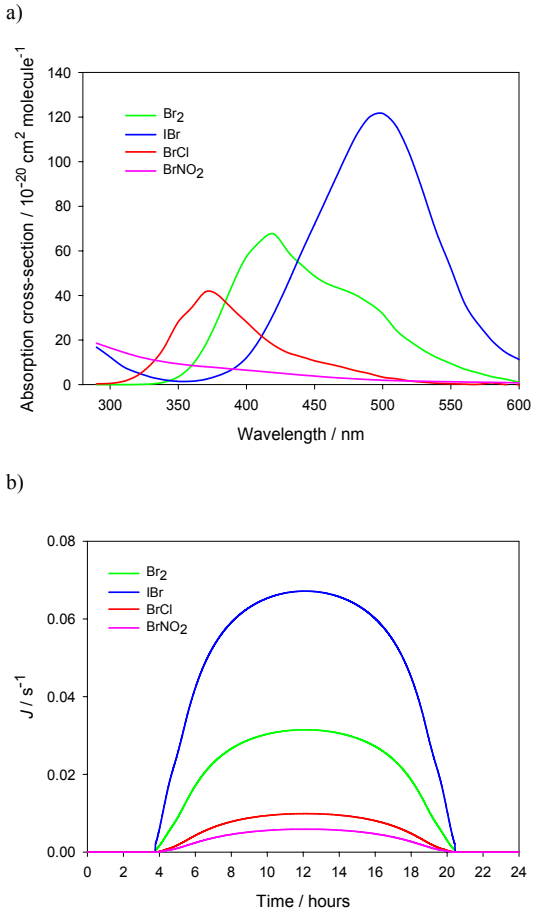

Fig. 10. (a) Absorption cross-sections of Br_2, BrCl, IBr and $BrNO_2$ as a function of wavelength. **(b)** Diurnal variation of the corresponding rates of photolysis, calculated assuming a quantum yield of unity for clear sky conditions at Mace Head in August.

ACPD
5, 9731–9767, 2005

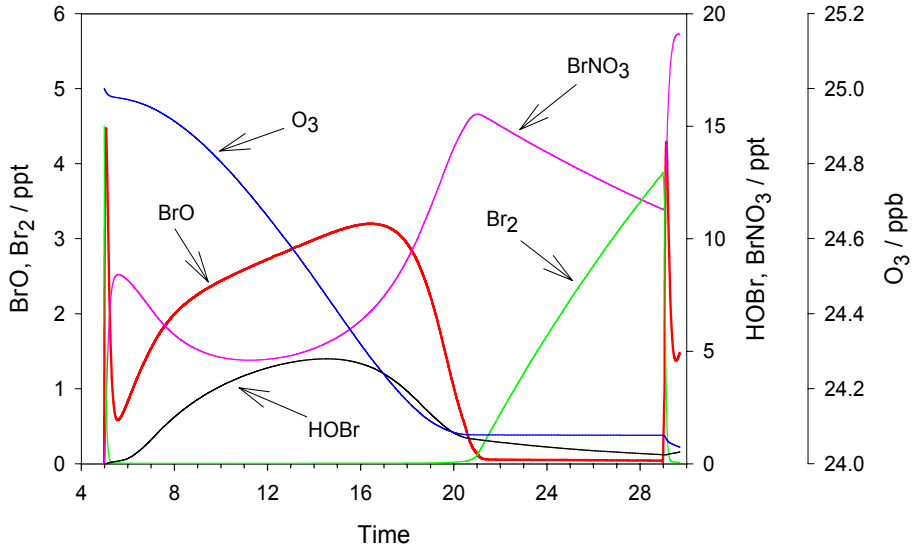

Fig. 11. Model simulation of the diurnal profiles of the main inorganic bromine species and O_3, for low NO_x conditions in the MBL.

ACPD
5, 9731–9767, 2005